# New Hybrid Materials Combining Nickel Bis(dithiolene) Metal Complexes and Reducible Stilbazolium Cations. A Search for Possible Interplay between Optical Nonlinearity and Conductivity

Isabelle Malfant, Nadège Cordente, Pascal G. Lacroix,* and Christine Lepetit

*Laboratoire de Chimie de Coordination du CNRS, 205 route de Narbonne, 31077 Toulouse Cedex, France*

*Received July 10, 1998. Revised Manuscript Received October 1, 1998*

The synthesis and crystal structure of a new compound of formula $(NOMS)^+[Ni(dmit)_2]^-$ is reported ($NOMS^+$ = 4′-nitro-1-methylstilbazolium, and $dmit^{2-}$ = 2-thioxo-1,3-dithiole-4,5-dithiolato). It crystallizes in triclinic space group $P\bar{1}$, $a = 10.029(1)$ Å, $b = 10.502(2)$ Å, $c = 13.051(2)$ Å, $\alpha = 106.57(2)°$, $\beta = 91.62(2)°$, $\gamma = 104.65(1)°$, $Z = 2$. $(NOMS)^+[Ni(dmit)_2]^-$ exhibits a powder conductivity in the range of $10^{-6}-10^{-5}$ S cm$^{-1}$, which is similar with that of $(DAMS)^+[Ni(dmit)_2]^-$ [$DAMS^+$ = 4′-(dimethylamino)-1-methylstilbazolium]. Contrary to $DAMS^+$, $NOMS^+$ undergoes a reversible reduction process at −770 mV (vs SCE). The second-order nonlinear optical properties of $NOMS^+$ are investigated versus $DAMS^+$ within the INDO−SOS formalism and versus $NOMS^0$, using molecular structures obtained from density functional theory (DFT) calculations. The data indicate a reversed charge-transfer process resulting in an enlarged hyperpolarizability after reduction of $NOMS^+$ into $NOMS^0$.

## Introduction

Molecular materials are a promising class of new materials that have emerged in many area of material science for designing new magnets,[1] molecular assemblies for data storage,[2] materials for nonlinear optics,[3−6] and conductors and superconductors.[7−9] The versatility of molecular chemistry offers a unique opportunity to meet additional challenges, such as designing multiproperty materials that would simultaneously possess several properties (e.g., magnetism and conductivity,[10,11] magnetism and nonlinear optical (NLO) properties,[12,13] or conductivity and NLO properties[14,15]) coupled in a possible interplay. Multifunctional materials are of current interest for their potential use in technologies where several properties need to be combined in the same device. For example, optoelectronics, in which electrons interface with photons, is expected to become increasingly important in the next few decades, for communication and all data processing.[16] This new frontier of science and technology could benefit from the design of new materials linking semiconductor-based electronics and NLO-based photonics, at the molecular level. Nevertheless, beside the possibility of future applications, the manipulation of light by electricity in a molecule is an intriguing challenge.

As part of our general research effort aimed at extending the range of molecular materials combining two properties in the same crystal, we have recently reported on hybrid compounds made of inorganic stacks of $[Ni(dmit)_2]^-$ anions ($dmit^{2-}$ = 2-thioxo-1,3-dithiole-4,5-dithiolato; Scheme 1), in which an organic NLO cation, 4′-(dimethylamino)-1-methylstilbazolium ($DAMS^+$; Scheme 1), was inserted.[17] The observation of short distances between chromophores and $[Ni(dmit)_2]^-$ species suggested that $\pi$-overlap between cations and anions could take place, resulting in a slight modifica-

(1) (a) Kahn, O. *Molecular Magnetism*; VCH: Weinheim, 1993. (b) Miller, J. S.; Epstein, A. J. *Angew. Chem., Int. Ed. Engl.* **1994**, *33*, 3, 385.
(2) Kahn, O.; Martinez, C. J. *Science* **1998**, *279*, 44.
(3) Optical Nonlinearities in Chemistry (special issue). *Chem. Rev.* **1994**, *94*.
(4) Prasad, P. N.; Williams, D. J. *Introduction to Nonlinear Optical Effects in Molecules and Polymers*; Wiley-Interscience: New York, 1991.
(5) *Materials for Nonlinear Optics: Chemical Perspectives;* Marder, S. R., Sohn, J. E., Stucky, G. D., Eds., ACS Symp. Ser. 445; American Chemical Society: Washington DC, 1991.
(6) Zyss J. *Molecular Nonlinear Optics;* Academic Press: New York, 1994.
(7) Cassoux, P.; Miller, J. S. In *Chemistry of Advanced Materials: An Overview*; Interrante, L. V., Hampden-Smith, M. J., Eds.; Wiley-VCH: New York, 1998; p 19.
(8) Special Issue on Molecular Conductors. *J. Mater. Chem.* **1995**, *5* (10).
(9) Williams, J. M.; Ferraro, J. R.; Thorn, R. J.; Carlson, K. D.; Geiser, U.; Wang, H. H.; Kini, A. M.; Whangbo, *Organic Superconductors (Including Fullerenes)*; Prentice Hall: Englewood Cliffs, NJ, 1992.
(10) Goze, F.; Laukhin, V. N.; Brossard, L.; Audouard, A.; Ulmet, J. P.; Askenazy, S.; Naito, T.; Kobayashi, H.; Kobayashi M.; Cassoux, P. *Europhys. Lett.* **1994**, *28*, 427.
(11) Kurmoo, M.; Graham, A. W.; Day, P.; Coles, S. J.; Hursthouse, M. B.; Caulfield, J. L.; Singleton, J.; Pratt, F. L.; Hayes, W.; Ducasse L.; Guionneau, P. *J. Am. Chem. Soc.* **1995**, *117*, 12209.
(12) (a) Clément, R.; Lacroix, P. G.; O′Hare D.; Evans, J. *Adv. Mater.* **1994**, *6*, 794. (b) Lacroix, P. G.; Clément, R.; Nakatani, K.; Zyss J.; Ledoux, I. *Science* **1994**, *263*, 658.
(13) Bernard, S.; Yu, P.; Coradin, T.; Rivière, E.; Nakatani, K.; Clément, R. *Adv. Mater.* **1997**, *9*, 981.
(14) Sutter, K.; Hulliger J.; Günter, P. *Solid State Commun.* **1990**, *74*, 867.
(15) Lacroix P. G.; Nakatani, K. *Adv. Mater.* **1997**, *9*, 1105.
(16) Dagani, R. *Chem. Eng. News* **1996**, March 4, 22.
(17) Malfant, I.; Andreu, R.; Lacroix, P. G.; Faulmann, C.; Cassoux, P. *Inorg. Chem.* **1998**, *37*, 3361.

10.1021/cm980487z CCC: $15.00 
Published on Web 12/03/1998

**Scheme 1**

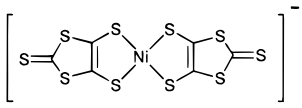

$[Ni(dmit)_2]^-$

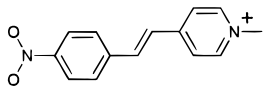

$NOMS^+$

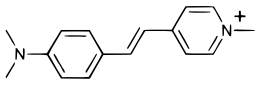

$DAMS^+$

tion of the overall electronic structure and hence the conductivity and the molecular hyperpolarizability ($\beta$) of the chromophores. However, this possibility, which offers a route toward an actual interplay between both properties, becomes more relevant when a subtle adjustment of the redox potentials of the anions and the cations is achieved. This condition was not observed in (DAMS)[Ni(dmit)$_2$], and we present here the second step of our investigation aimed at connecting $[Ni(dmit)_2]^-$ with more reducible cations. Among several possible candidate systems, we have selected the 4′-nitro-1-methylstilbazolium ($NOMS^+$; Scheme 1) species.

The organization of the paper will be the following: (i) The structure of the new (NOMS)[Ni(dmit)$_2$] compound will be described versus that of the already reported (DAMS)[Ni(dmit)$_2$] material. In a second section, (ii) the electronic structures will be discussed in relation with the redox properties of the chromophores. Then, (iii) the hyperpolarizability of $NOMS^+$ will be investigated versus that of $DAMS^+$, both experimentally (solvatochromism) and theoretically, within the INDO/SOS formalism on the basis of crystal data available. Finally, (iv) the possibility of tuning the NLO response of stilbazolium chromophore through a redox process will be investigated on the calculated structures of $NOMS^+$ and $NOMS^0$ obtained from the density functional theory (DFT).

## Experimental Section

**Starting Materials and Equipment.** Acetonitrile was purchased from SDS and distillated over $P_2O_5$ prior to use. $(n\text{-}Bu_4N)^+[Ni(dmit)_2]^-$ [18] and 4′-(dimethylamino)-1-methylstilbazolium iodide ($DAMS^+I^-$)[19]were synthesized as previously reported. Elemental analyses were performed by the "Service de Microanalyses du Laboratoire de Chimie de Coordination", in Toulouse, France. Electronic spectra were recorded on a Shimadzu UV 3100 spectrophotometer and $^1$H NMR on a Bruker AM 250 spectrometer. Electrochemical measurements were carried out with an Electrokemat potentiostat.[20]

**Table 1. Data Collection and Refinement for (NOMS)[Ni(dmit)$_2$]**

| | |
|---|---|
| formula | $C_{20}H_{13}N_2NiO_2S_{10}$ |
| $M_w$ | 692.65 |
| crystal form | diamond shape |
| crystal color | black |
| crystal size, (mm) | 0.22 × 0.20 × 0.05 |
| temp, K | 180 |
| crystal system | triclinic |
| space group | $P\bar{1}$ |
| $a$, Å | 10.029(1) |
| $b$, Å | 10.502(2) |
| $c$, Å | 13.051(2) |
| α, deg | 106.57(2) |
| $\beta$, deg | 91.62(2) |
| $\gamma$, deg | 104.65(1) |
| $V$, Å$^3$ | 1267.18 |
| $Z$ | 2 |
| $\rho$(calcd), g cm$^{-3}$ | 1.81 |
| $F_{000}$ | 704.83 |
| $\mu$ (Mo Kα), cm$^{-1}$ | 15.86 |
| diffractometer | IPdS Stoe |
| monochromator | graphite |
| radiation | Mo Kα ($\lambda$ = 0.71069 Å) |
| scan mode | $\phi$ |
| scan range $\phi$, deg | $0 < \phi < 250.5$ |
| $2\theta$ range, deg | $2.9 < 2\theta < 48.4$ |
| no. of measured reflns | 9890 |
| independent reflns (Rm) | 3662 (0.06) |
| intensities > 2 $\sigma(I)$ | 1896 |
| no. of parameters used | 317 |
| refinement on | $F$ |
| $R^a$ | 0.0303 |
| $R_w{}^b$ | 0.0342 |
| $S$ | 1.15 |

$^a$ $R = \sum(||F_o| - |F_c||)/\sum(|F_o|)$. $^b$ $R_w = \sum w(|F_o| - |F_c|)^2/\sum w(F_o)^2]^{1/2}$.

**Synthesis**. *NOMS$^+$I$^-$*. Following the general route first described by Philips,[21] 4-picoline (930 mg, $10^{-2}$ mol) and methyliodide (1.42 g, $10^{-2}$ mol) are readily reacted, which affords 4-picolinium iodide as a pale yellow solid. This resulting solid is dissolved in 15 mL of 2-propanol, with 1.51 g ($10^{-2}$ mol) of nitrobenzaldehyde and 3 drops of piperidine. The solution is refluxed overnight, and a brown yellow solid is obtained (3.36 g, yield 90%). A pure orange compound (yield 45%) is obtained after two recrystallizations in methanol. (Found: C, 44.62; H, 3.69; N, 7.21. Calcd for $C_{14}H_{13}IN_2O_2 \cdot {}^1/_2H_2O$: C, 44.58; H, 3.74; N, 7.43.) $^1$H NMR (250 MHz, DMSO-$d_6$, standard $SiMe_4$): $\delta$ 9.065 (2H, d, $J$ = 6.4 Hz), 8.472 (2H, d, $J$ = 8.6 Hz), 8.411 (2H, d, $J$ = 6.5 Hz), 8.242 (1H, d, $J$ = 16.4 Hz), 8.122 (2H, d, $J$ = 8.6 Hz), 7.875 (1H, d, $J$ = 16.4 Hz), 4.412 (3H, s). To avoid problems related to the presence of iodide, a potential reducing agent for the electrochemical study, the $NOMS^+PF_6^-$ salt was prepared by metathesis with an excess of $KPF_6$ in a MeOH/$H_2O$ mixture containing $NOMS^+I^-$. (Found: C, 43.11; H, 2.88; N, 7.10. Calcd for $C_{14}H_{13}F_6N_2O_2P$: C, 43.54; H, 3.39; N, 7.25.)

Single crystals of (NOMS)[Ni(dmit)$_2$] were obtained by slow interdiffusion of a saturated solution of $(n\text{-}Bu_4N)^+[Ni(dmit)_2]^-$ and $NOMS^+PF_6^-$. These experiments were carried out under argon, in a three-compartment H-tube equipped with porous glass frits between the compartments. The concentration of the solutions was kept close to saturation during the diffusion process by means of additional porous containers placed in the appropriate compartment and filled with an excess of solid starting reagents.

**Structure Analysis and Refinement.** The structures were solved by direct methods (Shelxs-86)[22] and refined by least-squares procedures. Crystallographic data for (NOMS)-[Ni(dmit)$_2$] are summarized in Table 1. The calculations were

(18) (a) Steimecke, G.; Sieler, H. J.; Kirmse R.; Hoyer, E. *Phosphorous Sulfur* **1979**, *7*, 49. (b) Valade, L.; Legros, J. P.; Bousseau, M.; Cassoux, P.; Garbauskas M.; Interrante, L. *J. Chem. Soc., Dalton Trans.* **1985**, 783.

(19) Kung, T. K. *J. Chin. Chem. Soc.* **1978**, *25*, 131.

(20) Cassoux, P.; Dartiguepeyron, R.; de Montauzon, D.; Tommasino, J. B.; Fabre, P. L. *Actual. Chim.* **1994**, *1*, 49.

(21) Phillips, A. P. *J. Org. Chem.* **1947**, *12*, 333.

(22) Sheldrick, G. M. *SHELXS86, Program for Crystal Structure Solution*; University of Göttingen: Göttingen, Germany, 1986.

carried out with the CRYSTALS package of programs[23] running on a PC. The drawings of the molecular structures were obtained with the help of CAMERON.[23] The atomic scattering factors were taken from *International Tables for X-ray Crystallography*.[24] Full X-ray data, fractional atomic coordinates, and equivalent thermal parameters for all atoms and anisotropic thermal parameters have been deposited at the Cambridge Crystallographic Data Center.

**Conductivity.** Powder conductivity measurements were carried out on pressed pellets of pure powder materials (size: 1 mm$^2$ × about 1 mm) obtained by careful grinding. The cylinders used to press the materials were used as electrodes.

**Electrochemistry.** Electrochemical measurements were carried out in an airtight three-electrode cell connected to a vacuum argon/$N_2$ line, using the interrupt method to minimize the uncompensated resistance (iR) drop. Cyclic voltammetry was recorded in acetonitrile, with $Bu_4N^+PF_6^-$ as supporting electrolyte (0.1 mol L$^{-1}$). The working electrode was platinum, and a saturated calomel electrode (SCE) was used as a reference. The scan rate was 30 mV s$^{-1}$. Electrolysis was performed at −1000 mV using platinum foil as a working electrode.

**Computational Details.** All geometries were fully optimized using the Gaussian94 program package[25] within the framework of DFT at the B3PW91/6-31G* level.

The all-valence INDO/S (intermediate neglect of differential overlap) method,[26] in connection with the sum-over-state (SOS) formalism,[27] was employed for the calculation of the molecular hyperpolarizability of NOMS$^+$ and DAMS$^+$. Structural parameters used for the INDO calculations were taken from the present crystal study for [NOMS][Ni(dmit)$_2$] and from the previously reported structure for [DAMS][Ni(dmit)$_2$].[17] Details of the computationally efficient INDO−SOS-based method for describing second-order molecular optical nonlinearities have been reported elsewhere.[28] Calculation was performed using the INDO/1 Hamiltonian incorporated in the commercially available MSI software package ZINDO.[29] The monoexcited configuration interaction (MECI) approximation was employed to describe the excited states. The 100 energy transitions between the 10 highest occupied molecular orbitals and the 10 lowest unoccupied ones were chosen to undergo CI mixing.

Static hyperpolarizabilities of the calculated structure of NOMS$^+$ and NOMS$^0$ were evaluated using the numerical finite field procedures included in MOPAC 6.00-PM3[30] or in Gaussian94.[25] A field strength ($E$) of 0.001 au was chosen for both the cationic and neutral species (we have checked that $\beta$ does not depend on $E$ in the $5 \times 10^{-3}$−$10^{-4}$ range). The Coupled Perturbed Hartree−Fock (CPHF) procedure available in Gaussian 94 was also used.

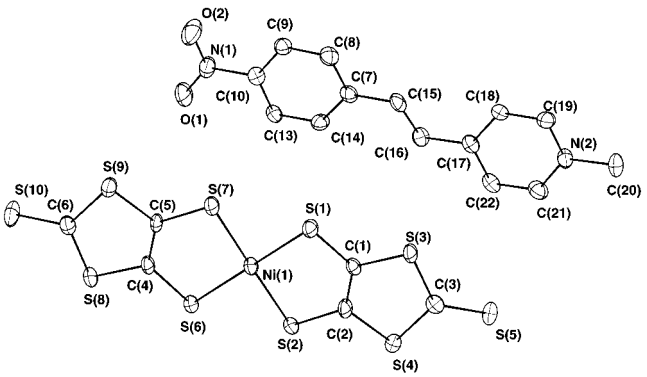


**Figure 1.** Atom labeling scheme for (NOMS)[Ni(dmit)$_2$].

**Table 2. Atomic Coordinates and Equivalent Isotropic Displacement Parameters for (NOMS)[Ni(dmit)$_2$][a]**

| atom | *x/a* | *y/b* | *z/c* | *U*(eq) |
|---|---|---|---|---|
| Ni(1) | 0.12402(9) | 0.37189(8) | 0.48919(6) | 0.0246 |
| S(1) | 0.2277(2) | 0.5843(1) | 0.5031(1) | 0.0288 |
| S(2) | 0.0956(2) | 0.4202(1) | 0.6594(1) | 0.0280 |
| S(3) | 0.2987(2) | 0.8433(1) | 0.6939(1) | 0.0296 |
| S(4) | 0.1764(2) | 0.6936(1) | 0.8383(1) | 0.0329 |
| S(5) | 0.3186(2) | 0.9956(2) | 0.9266(1) | 0.0427 |
| S(6) | 0.0178(2) | 0.1599(1) | 0.4742(1) | 0.0280 |
| S(7) | 0.1589(2) | 0.3252(1) | 0.3207(1) | 0.0308 |
| S(8) | −0.0500(2) | −0.0978(1) | 0.2812(1) | 0.0307 |
| S(9) | 0.0767(2) | 0.0532(1) | 0.1389(1) | 0.0320 |
| S(10) | −0.0525(2) | −0.2511(2) | 0.0515(1) | 0.0452 |
| C(1) | 0.2251(6) | 0.6664(5) | 0.6367(4) | 0.0229 |
| C(2) | 0.1689(6) | 0.5957(5) | 0.7043(4) | 0.0266 |
| C(3) | 0.2675(7) | 0.8544(6) | 0.8269(5) | 0.0308 |
| C(4) | 0.0233(6) | 0.0787(5) | 0.3404(4) | 0.0239 |
| C(5) | 0.0820(6) | 0.1494(5) | 0.2732(4) | 0.0238 |
| C(6) | −0.0109(6) | −0.1052(6) | 0.1517(4) | 0.0280 |
| C(7) | 0.5955(6) | 0.7477(6) | 0.3882(4) | 0.0270 |
| C(8) | 0.6021(7) | 0.7439(6) | 0.2798(4) | 0.0310 |
| C(9) | 0.5717(6) | 0.6195(6) | 0.1975(4) | 0.0279 |
| C(10) | 0.5305(6) | 0.4987(6) | 0.2247(4) | 0.0258 |
| C(13) | 0.5214(6) | 0.4974(5) | 0.3304(4) | 0.0271 |
| C(14) | 0.5556(6) | 0.6214(6) | 0.4112(4) | 0.0276 |
| C(15) | 0.6321(7) | 0.8799(5) | 0.4735(5) | 0.0289 |
| C(16) | 0.6259(6) | 0.8996(6) | 0.5768(4) | 0.0267 |
| C(17) | 0.6653(6) | 1.0353(5) | 0.6606(4) | 0.0251 |
| C(18) | 0.7208(6) | 1.1598(5) | 0.6368(4) | 0.0276 |
| C(19) | 0.7565(6) | 1.2825(6) | 0.7168(4) | 0.0298 |
| C(20) | 0.7815(7) | 1.4239(6) | 0.9060(5) | 0.0378 |
| C(21) | 0.6823(7) | 1.1724(6) | 0.8461(5) | 0.0345 |
| C(22) | 0.6471(6) | 1.0460(6) | 0.7676(5) | 0.0299 |
| N(1) | 0.4951(6) | 0.3659(5) | 0.1395(4) | 0.0361 |
| N(2) | 0.7375(5) | 1.2887(5) | 0.8202(4) | 0.0299 |
| O(1) | 0.4547(5) | 0.2600(4) | 0.1651(3) | 0.0455 |
| O(2) | 0.5108(6) | 0.3663(5) | 0.0466(3) | 0.0578 |

[a] Esds in parentheses refer to the last significant digit. *U*(eq) is defined as the arithmetic mean of $U_{ii}$.

## Results and Discussion

**Description of the Structure of (NOMS)[Ni(dmit)$_2$].** The molecular structure is shown in Figure 1 with the atomic numbering scheme employed, while atomic coordinates are gathered in Table 2. The asymmetric unit consists of one planar [Ni(dmit)$_2$]$^-$ entity (largest deviation from planarity 0.115 Å at S(5)) and one NOMS$^+$ cation. No atom is on a special position. A collection of some relevant intramolecular distances is given in Table 3 for the [Ni(dmit)$_2$]$^-$ species. The mean Ni−S distance is 2.168(2) Å, which is somewhat larger than those observed for other compounds of general formula [Cat]$^+$[Ni(dmit)$_2$]$^-$, where [Cat]$^+$ is a closed-shell cation. For comparison, the Ni−S distances observed for [Cat]$^+$ = [NMe$_4$]$^+$, [NEt$_4$]$^+$, [NPr$_4$]$^+$, and

(23) (a) Watkin, D. J.; Prout, C. K.; Carruthers, J. R.; Betteridge, P. W. *CRYSTALS Issue 10*, Chemical Crystallography Laboratory, University of Oxford: Oxford, 1996. (b) Watkin, D. J.; Prout, C. K.; Pearce, L. J. *CAMERON*, Chemical Crystallography Laboratory, University of Oxford: Oxford, 1996.

(24) Cromer, D. T.; Waber, J. T. *International Tables for X-ray Crystallography*; Kynoch Press: Birmingham, 1974; Vol. 4.

(25) Frisch, M. J.; Trucks, G. W.; Schlegel, H. B.; Gill, P. M. W.; Johnson, B. G.; M. Robb, M. A.; Cheeseman, J. R.; Keith, T.; Petersson, G. A.; Montgomery, J. A.; Raghavachari, K.; Al-Laham, M. A.; Zakrzewski, V. G.; Ortiz, J. V.; Foresman, J. B.; Cioslowski, J.; Stefanov, B. B.; Nanayakkara, A.; Challacombe, M.; Peng, C. Y.; Ayala, P. Y.; Chen, W.; Wong, M. W.; Andres, J. L.; Replogle, E. S.; Gomperts, R.; Martin, R. L.; Fox, D. J.; Binkley, J. S.; Defrees, D. J.; Baker, J.; Stewart, J. P.; Head- Gordon, M.; Gonzalez, C.; Pople. J. A. *Gaussian 94, Revision E.2*, Gaussian, Inc.: Pittsburgh, PA, 1995.

(26) (a) Zerner, M.; Loew, G.; Kirchner, R.; Mueller-Westerhoff, U. *J. Am. Chem. Soc.* **1980**, *102*, 589. (b) Anderson, W. P.; Edwards, D; Zerner, M. C. *Inorg. Chem.* **1986**, *25*, 5, 2728.

(27) Ward, J. F. *Rev. Mod. Phys.* **1965**, *37*, 1.

(28) Kanis, D. R.; Ratner, M. A.; Marks, T. J. *Chem. Rev.* **1994**, *94*, 195.

(29) ZINDO, 96.0/4.0.0., Molecular Simulations Inc., 1996.

(30) (a) MOPAC 6.00: Stewart, J. J. P. *QCPE* no. 455. (b) Stewart, J. J. P. *J. Comput. Chem.* **1989**, *10*, 209.

**Table 3. Selected Bond Lengths for (NOMS)[Ni(dmit)$_2$] (in Å)**

| | | | |
|---|---|---|---|
| Ni(1)−S(1) | 2.162(2) | S(1)−C(1) | 1.714(5) |
| Ni(1)−S(2) | 2.178(2) | S(2)−C(2) | 1.719(5 |
| Ni(1)−S(6) | 2.160(2) | S(6)−C(4) | 1.721(5) |
| Ni(1)−S(7) | 2.171(2) | S(7)−C(5) | 1.729(5) |

$[NBu_4]^+$ are 2.158(3),[31] 2.157(4),[32] 2.160(3),[31] and 2.156[33] Å, respectively. However, this result is in agreement with the situation encountered in $[C_6H_{11}N_2]^+[Ni(dmit)_2]^-$ reported by Reedijk et al.[34] According to these authors, the overall electronic structure of $[Ni(dmit)_2]^-$ may be slightly modified through possible $\pi$-overlap between the orbitals of a $\pi$-conjugated cations with those of the anions, which results in an increased Ni−S distance. This situation is observed in $(NOMS)^+[Ni(dmit)_2]^-$ as in the previously reported $(DAMS)^+[Ni(dmit)_2]^-$ (mean Ni−S distance = 2.159(1) and 2.164(1) Å for phases **3** and **4,** respectively).[17]

Before going further in the description of $(NOMS)^+[Ni(dmit)_2]^-$, it is worthwhile to note that the parent $(DAMS)^+[Ni(dmit)_2]^-$ exhibits two phases. One of them, monoclinic space group $P2_1/c$ (phase **3**) consists of alternating chains of $[Ni(dmit)_2]^-$ anions, while the other one, triclinic space group $P\bar{1}$ (phase **4**) exhibits the same general structural features as for the present $(NOMS)^+[Ni(dmit)_2]^-$. Therefore, any comparison between both materials will be based on the triclinic phases only. A projection of the structure onto the *ab* plane for $(DAMS)^+[Ni(dmit)_2]^-$ and onto the (011) plane for $(NOMS)^+[Ni(dmit)_2]^-$ is shown in Figure 2. It reveals that the $[Ni(dmit)_2]^-$ species are organized in layers through short S···S intermolecular contacts (<3.7 Å) in both structures. The lengths of the S···S contacts are gathered in Table 4 for $(NOMS)^+[Ni(dmit)_2]^-$ and are somewhat comparable with the situation encountered for $(DAMS)^+[Ni(dmit)_2]^-$. The $NOMS^+$ cations are almost planar, with an angle of 7.1° between the *N*-methylpyridyl and the *p*-nitrophenyl fragments. The major difference is observed in the way the cationic species are inserted between the sulfur layers. While $DAMS^+$ lies roughly perpendicular to $[Ni(dmit)_2]^-$ (angle between averaged molecular planes, 85.3°), $NOMS^+$ and $[Ni(dmit)_2]^-$ are almost parallel to $(NOMS)[Ni(dmit)_2]$, with an angle of 9.9° between the molecular planes. This situation, which favors $\pi$-overlaps between ions, may strongly influence the electronic structure of the material (vide infra).

**Electronic Structure of (NOMS)[Ni(dmit)$_2$] versus (DAMS)[Ni(dmit)$_2$].** The conductivities of $(NOMS)[Ni(dmit)_2]$ and $(DAMS)[Ni(dmit)_2]$ recorded on powder samples are in the range $10^{-5}$−$10^{-6}$ S cm$^{-1}$. Due to the small size of the crystals, it was impossible to check the temperature dependence of the conductivity of crystals. The powder conductivity values suggest a semiconducting behavior, as expected for integral oxidation state 1:1 salts. Indeed, most of the 1:1 salts of $[Ni(dmit)_2]^-$ with closed-shell type cations such as $NR_4^+$ (R = alkyl) or $SMe_xEt_{3-x}^+$ ($x$ = 1, 2, 3) exhibit conductivities lower than $10^{-5}$ S cm$^{-1}$. In fact, 1:1 salts with open-shell cation, such as 1,2,3-trimethylimidazolium, have been observed to exhibit enhanced conductivities, but the semiconducting behavior remains.[34] Therefore, the intrinsic behavior of $(NOMS)^+[Ni(dmit)_2]^-$ is probably semiconducting.

The origin of the conductivity of $(DAMS)^+[Ni(dmit)_2]^-$ has been thoroughly discussed in our previous study[17] in term of short S···S contacts between $[Ni(dmit)_2]^-$ units, the cation not being involved in the electronic properties of the material. The role of the S···S short distances (Table 4) in the conductivity of $(NOMS)[Ni(dmit)_2]$ can be tentatively understood from the examination of the crystal structure. These contacts correspond to a possible two-dimensional path of conductivity in the *bc* plane. Most of them are observed between $[Ni(dmit)_2]^-$ entities related by the symmetry operation (*i*). They are associated with $\pi$-overlaps of $\pi$-orbitals and, hence, modest transfer integrals (Table 5). These values are on the same order of magnitude than those already calculated for $(DAMS)^+[Ni(dmit)_2]^-$ and are consistent with the modest conductivities recorded for both 1:1 salts.

The cations have not been taken into account in the above discussion of the origin of the conductivity. Actually, cations with delocalized $\pi$-systems have the potential to modify the overall electronic structure of the material, which should result in changes in conductivity and hyperpolarizability. Increasing the number of short contacts would likely favor electron delocalizations, which offer a route for linking NLO and conducting properties. It is interesting to note that several short distances are observed in the crystal structures of $(NOMS)[Ni(dmit)_2]$ (Table 6). $(DAMS)[Ni(dmit)_2]$ exhibits the same structural features, but to a far less extent: one short distance instead of seven. In conclusion, from a structural point of view, $(NOMS)[Ni(dmit)_2]$ seems to be more suitable than $(DAMS)[Ni(dmit)_2]$ for achieving a link and, hence, a possibility of interplay between NLO and conductivity.

On the other hand, an important prerequisite for electron transfer from the anions to the cations implies an adjustment of the redox properties of both species. Electrochemical data of $DAMS^+PF_6^-$ and $NOMS^+PF_6^-$ are summarized in Table 7 and illustrated in Figure 3 for $NOMS^+PF_6^-$. $DAMS^+$ undergoes an irreversible reduction process at $E^{1/2}$ = −1080 mV in a potential range far below the 290 mV value reported for the oxidation of the $[Ni(dmit)_2]^-$ species. Consequently, although short contacts are evidenced between cations and anions in the crystal structure of $(DAMS)[Ni(dmit)_2]$, a difference in potential of 1370 mV is much beyond the limit value of 250 mV proposed by Wheland for obtaining charge delocalization.[35] Such a potential barrier prohibits any electronic communication between cations and anions. The situation encountered for $NOMS^+$ is more favorable for $\pi$-interactions and extension of the electronic effects, with a redox potential of −770 mV (averaged cathodic and anodic peak potentials) and reversible redox behavior, as indicated by the $\Delta E$ value around 60 mV. However, this shift of 310 mV is not fully sufficient to allow any observable electron

(31) van Diemen, J. H.; Groeneveld, L. R.; Lind, A.; de Graaff, R. A. G.; Haasnoot, J. G.; Reedijk, J. *Acta Crystallogr.* **1988**, *C44*, 1898.
(32) Groeneveld, L. R.; Schuller, B.; Kramer, G. J.; Haasnoot, J. G.; Reedijk, J. *Recl. Trav. Chim. Pays-Bas* **1986**, *105*, 507
(33) Lindqvist, O.; Andersen, L.; H. J. Sieler, G. Steimecke and E. Hoyer, *Acta Chem. Scand. Ser.* **1982**, *A36*, 855.
(34) Reefman, D.; Cornelissen, J. P.; Haasnoot, J. G.; de Graaff R. A. G.; Reedijk, J. *Inorg. Chem.* **1990**, *29*, 3933.
(35) Wheland, R. C. *J. Am. Chem. Soc.* **1976**, *98*, 3926.

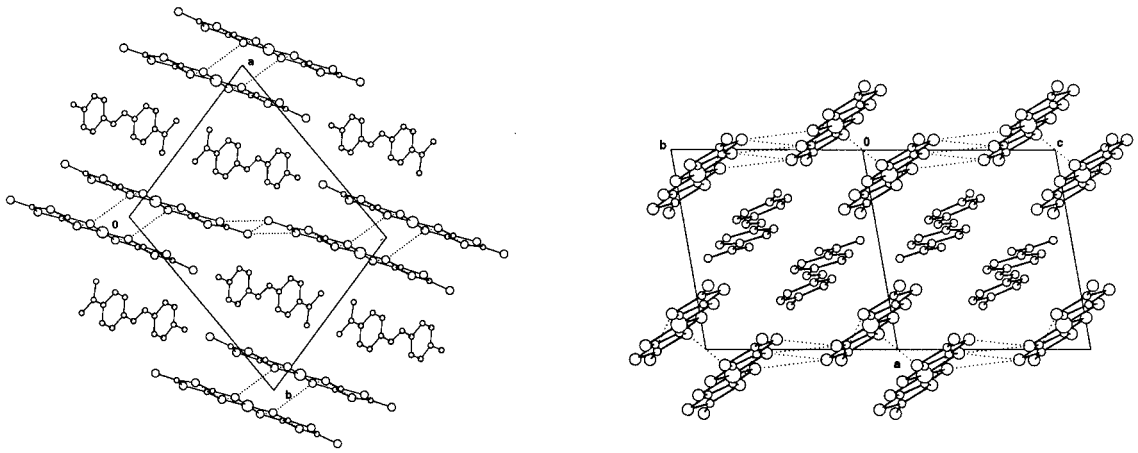

**Figure 2.** Projection of (DAMS)[Ni(dmit)$_2$] onto the *ab* plane (left) and (NOMS)[Ni(dmit)$_2$] onto the (011) plane (right). The dotted lines represent the S···S distances shorter than the sum (3.7 Å) of the van der Waals radii.

**Table 4. S···S Intermolecular Contacts (<3.7 Å) for (NOMS)[Ni(dmit)$_2$] versus (DAMS)[Ni(dmit)$_2$]**

| (NOMS)[Ni(dmit)$_2$] | | (DAMS)[Ni(dmit)$_2$] | |
|---|---|---|---|
| atoms[a] | distances | atoms[b] | distances |
| S(2)−S(8i) | 3.607(1) | S(1)−S(2i) | 3.663(1) |
| S(6)−S(6i) | 3.545(1) | S(1)−S(6i) | 3.491(1) |
| S(6)−S(8i) | 3.458(1) | S(7)−S(6i) | 3.661(1) |
| S(9)−S(9ii) | 3.642(1) | S(3)−S(2i) | 3.618(1) |
| S(4)−S(10iii) | 3.669(1) | S(7)−S(8i) | 3.602(1) |
| | | S(1)−S(7ii) | 3.699(1) |
| | | S(4)−S(5iv) | 3.608(1) |
| | | S(5)−S(5v) | 3.670(2) |

[a] Symmetry operations for second atom: (i) $-x, -y, 1-z$; (ii) $-x, -y, -z$; (iii) $x, 1+y, 1+z$. [b] Symmetry operations for second atom: (i) $x, y, z-1$; (ii) $2-x, 2-y, -z$; (iii) $1-x, 1-y, -z$; (iv) $1-x, 1-y, -1-z$; (v) $2-x, 2-y, 1-z$.

**Table 5. Transfer Integrals (in eV) Calculated for the Partially Filled [Ni(dmit)$_2$]$^-$ Orbital (orbital 48) in Several Direction for (NOMS)[Ni(dmit)$_2$] versus (DAMS)[Ni(dmit)$_2$]**

| direction | symmetry operation[a] | transfer integral |
|---|---|---|
| | (NOMS)[Ni(dmit)$_2$] | |
| *bc* plane | i | 0.0055 |
| [001] | ii | 0.0022 |
| [011] | iii | 0.0056 |
| | (DAMS)[Ni(dmit)$_2$] | |
| *ab* plane | i | 0.0059 |
| | ii | 0.0375 |
| | iii | 0.0019 |
| | iv | 0.0035 |
| | v | 0.0360 |

[a] Symmetry operations are labeled according to Table 4.

interaction, even if an increased number of short distances between cations and anions suggests that some progress has been made toward this goal.

**Hyperpolarizability of NOMS$^+$ versus DAMS$^+$.** The most traditional method for measuring the hyperpolarizability of a second-order NLO chromophore is the electric field induced second-harmonic generation (EFISH) technique. This approach, which requires poling the chromophores with electric fields, is inoperative for ionic species such as NOMS$^+$ and DAMS$^+$. A new technique based on Hyper-Rayleigh Scattering (HRS) has become an alternative method for measuring the hyperpolarizabilities of charged chromophores.[36] However, this technique has shown some inconstancy; for example, multiphoton fluorescence often interferes

**Table 6. Short Intermolecular Distances (<3.6 Å) between Cations and Anions (in Å) for (NOMS)[Ni(dmit)$_2$] and (DAMS)[Ni(dmit)$_2$]**

| atoms | distances, Å | symmetry operations |
|---|---|---|
| | (NOMS)[Ni(dmit)$_2$] | |
| S(9)−C(22) | 3.500(1) | $1-x, 1-y, 1-z$ |
| S(1)−C(19) | 3.524(1) | $1-x, 2-y, 1-z$ |
| S(2)−C(19) | 3.534(1) | $x-1, y-1, z$ |
| S(8)−C(8) | 3.462(1) | $x-1, y-1, z$ |
| S(10)−C(20) | 3.359(1) | $x-1, y-2, z-1$ |
| S(1)−C(14) | 3.500(1) | $x, y, z$ |
| S(3)−C(22) | 3.541(1) | $x, y, z$ |
| | (DAMS)[Ni(dmit)$_2$] | |
| S(6)−C(11) | 3.564(1) | $x, 1+y, 1+z$ |

**Table 7. Electrochemical Data for DAMS$^+$ and NOMS$^+$[a]**

| | $E_1$ | | | $E_2$ | | |
|---|---|---|---|---|---|---|
| | $E_{red}$ | $E_{ox}$ | ($\Delta E$) | $E_{red}$ | $E_{ox}$ | ($\Delta E$) |
| DAMS$^+$ | −1080 (irreversible) | | | | | |
| NOMS$^+$ | −810 | −730 | (80) | −885 | −830 | (55) |

[a] $E_1$ and $E_2$ (in mV vs SCE) correspond to the NOMS$^+$/NOMS$^0$ and NOMS$^0$/NOMS$^-$ redox potentials, respectively.

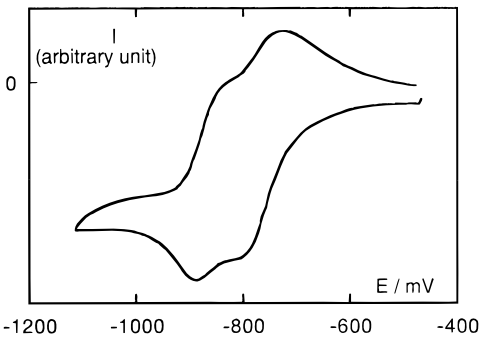


**Figure 3.** Cyclic voltammogram for NOMS$^+$PF$_6$- in acetonitrile.

and this can lead to serious experimental errors.[37,38] On the other hand, spectroscopy provides a simple approach based on solvatochromic shifts, which are indicative of changes in dipole moments ($\Delta\mu$) upon electronic excita-

(36) (a) Clays, K.; Persoons, A. *Phys. Rev. Lett.* **1991**, *66*, 2980. (b) Clays, K.; Persoons, A. *Rev. Sci. Instrum.* **1992**, *63*, 3285.

(37) Flipse, M. C.; de Jonge, R.; Woudenberg, R. H.; Marsman, A. W.; van Walree, C. A.; Jenneskens, L. W. *Chem. Phys. Lett.* **1995**, *245*, 297.

(38) Song, N. W.; Kang, T.-I.; Jeoung, S. C.; Jeon, S.-J.; Cho, B. R.; Kim, D. *Chem. Phys. Lett.* **1996**, *261*, 307.

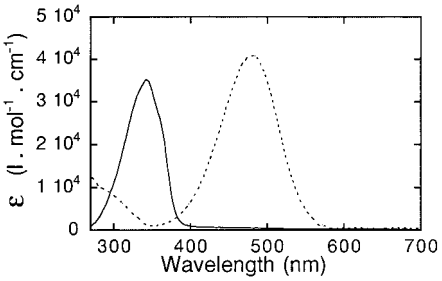


**Figure 4.** Electronic absorption spectra for $NOMS^+I^-$ recorded in EtOH. $DAMS^+I^-$ (dotted line) is shown as a reference.

tions. According to the well-known and widely used "two-level model",[39] the hyperpolarizability ($\beta$) of "push-pull" stilbazolium dyes is well-described in terms of a ground and an excited state having charge-transfer character and is related to the energy of the optical transition ($E$), its oscillator strength ($f$), and the difference between ground and excited-state dipole moment ($\Delta\mu$) through the relation:

$$\beta \propto f\Delta\mu/E^3$$

Therefore, large solvatochromism is strongly indicative of a large hyperpolarizability. The UV−visible spectra of $NOMS^+I^-$ and $DAMS^+I^-$ recorded in ethanol are compared in Figure 4. Both chromophores exhibit intense low lying transitions located at 343 nm ($\epsilon$ = 35200 $mol^{-1}$ L $cm^{-1}$) and 481 nm ($\epsilon$ = 40800 $mol^{-1}$ L $cm^{-1}$) for $NOMS^+I^-$ and $DAMS^+I^-$, respectively. The oscillator strengths can be extracted from the spectra through the relation:[40]

$$f = 4.315 \times 10^{-9} \int \epsilon \, d\nu$$

where the integration extends over the entire absorption band and $\nu$ is the wavenumber ($cm^{-1}$). Using the above relation leads to $f$ = 0.77 and 0.68 for $NOMS^+$ and $DAMS^+$, respectively. In the case of $NOMS^+$, it must be noted that the intense band centered at 343 nm exhibits a slight shoulder located at lower frequency. This effect, which becomes important at higher concentration, may be related to intermolecular interactions. Such behavior is well-documented for cationic dyes[41−44] and has been reported as characteristic of J aggregates (or Scheibe aggregates).[45] However, no further investigations were performed to clarify this question.

The energy maxima ($\lambda_{max}$) of both chromophores recorded in solvent of different polarities are compared in Table 8. The negative solvatochromism (red shift as the solvent polarity is decreasing) in $DAMS^+I^-$ is also observed in $NOMS^+I$, but to a lesser extent, as anticipated for a reduced "push-pull" character. These differences are shown in Figure 5, where the energy transition ($\nu$, $cm^{-1}$) is drawn versus the Reichardt solvent parameter $E_T^N$.[46] Because $NOMS^+$ and $DAMS^+$ have very closely related molecular structures, we make the assumption that comparing $\Delta\lambda$ for both chromophores can account for $\Delta\mu$. Therefore, $\Delta\mu$ should be roughly proportional to the slopes of the curves in Figure 5. According to the two-level model, the above $E$, $f$, and $\Delta\mu$ values strongly suggest a large decrease of $\beta$, while passing from $DAMS^+$ to $NOMS^+$. This effect is not surprising. It has long been recognized that the effects of substituent patterns on the hyperpolarizability of a chromophore are correlated with the electron-donating and -accepting strength of the substitutents. In other words, while the dimethylamino group is expected to enlarge the NLO response by increasing the intramolecular charge transfer and lowering its energy in $DAMS^+$, this effect is inoperative in $NOMS^+$, which should therefore exhibit a much reduced NLO response. The experimental values fit the relation:

$$\beta_{NOMS^+} = 0.252\beta_{DAMS^+}$$

This order of magnitudes in the hyperpolarizabilities is also supported by theoretical calculations. The calculated $\beta$ values of $NOMS^+$ and $DAMS^+$ are reported in Table 9. The data illustrate the well-known tendency for $\beta$ enhancement when the second harmonic is close to the absorption maxima. As anticipated from the electronic spectra and solvatochromic behavior, $\beta$ is deeply reduced in magnitude, upon changing the dimethylamino to a nitro substituent, but $NOMS^+$ still exhibits a sizable NLO response. The static $\beta$ values, which are the intrinsic hyperpolarizabilities calculated at zero frequency, are the data to be compared with the

**Table 8. Absorption Maxima ($\lambda_{max}$ in nm) of the Lowest Energy Optical Transition for $NOMS^+I^-$ and $DAMS^+I^-$, in Solvents of Different Polarities**

| | $NOMS^+I^-$ | $DAMS^+I^-$ | $E_T^N$ [a] |
|---|---|---|---|
| THF | 346 | 476 | 0.207 |
| pyridine | 352 | 493 | 0.293 |
| DMSO | 352 | 470 | 0.441 |
| EtOH | 344 | 481 | 0.654 |
| MeOH | 342 | 475 | 0.765 |
| $H_2O$ | 332 | 449 | 1.000 |

[a] Reichardt empirical solvent parameter (ref 46).

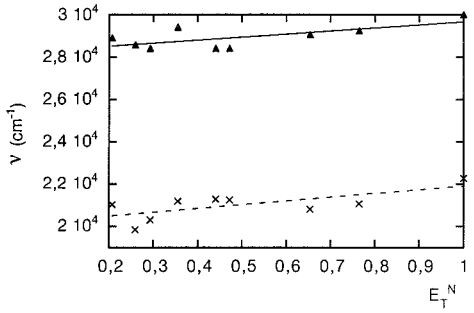


**Figure 5.** Solvatochromism of $NOMS^+$ versus $DAMS^+$ (dotted line) according to Table 8. The slopes (−34 and −21 for $DAMS^+$ and $NOMS^+$, respectively) indicate a reduced $\Delta\mu$ in $NOMS^+$.

(39) (a) Oudar, J. L.; Chemla, J. *J. Chem. Phys.* **1977**, *66*, 2664. (b) Oudar, J. L., *J. Chem. Phys.* **1977**, 67, 446.
(40) Orchin, M.; Jaffé, H. H. *Symmetry Orbitals, and Spectra*; John Wiley: New York, 1971; p 204.
(41) Dietz, F. In *Polymethine Dyes−Structure and Properties*; Tyutyulkov, N., Ed.; St. Kliment Ohridski University Press: Sofia, 1991; p 107.
(42) Coradin, T.; Clément, R.; Lacroix, P. G.; Nakatani, K. *Chem. Mater.* **1996**, *8*, 2153.
(43) Dähne, L. *J. Am. Chem. Soc.* **1995**, *117*, 12855.
(44) De Rossi, U.; Dähne, S.; Meskers, S. C. J.; Dekkers, H. P. J. M. *Angew. Chem. Int. Ed. Engl.* **1996**, *35*, 760.
(45) Möbius, D. *Adv. Mater.* **1995**, *7*, 437.
(46) Reichardt, C.; Harbush-Görnet, E. *Liebigs Annal. Chem.* **1983**, *5*, 721.

**Table 9. Molecular Hyperpolarizability ($\beta_{Tot} = \beta_{-2} + \beta_{-3}$) Calculated as a Function of the Laser Wavelength for NOMS⁺ and DAMS⁺**

| | hyperpolarizability ($10^{-30}$ cm$^5$ esu$^{-1}$) | | | |
|---|---|---|---|---|
| | NOMS⁺ | | DAMS⁺ | |
| wavelength ($\mu$m) | $\beta_{tot}$ | $(\beta_2 + \beta_{-3})$ | $\beta_{tot}$ | $(\beta_2 + \beta_{-3})$ |
| ∞[a] | −16.7 | (−54.4 + 37.7) | −98.2 | (−157.2 + 59.5) |
| 1.907 | −22.0 | (−64.6 + 42.6) | −139.1 | (−209.8 + 71.3) |

[a] ∞ stands for the infinite wavelength (static hyperpolarizability).

**Table 10. INDO Calculated Energies ($\lambda_{max}$ in nm), Oscillator Strengths ($f$), Dipole Moment Changes between Ground and Excited State ($\Delta\mu$ in D), and Composition of the First Excited State NOMS⁺ and DAMS⁺**

| compd | transition | $\lambda_{max}$ | f | $\Delta\mu$ | composition[a] of CI expansion |
|---|---|---|---|---|---|
| NOMS⁺ | 1→4 | 360 | 1.20 | −12.0 | 0.956 $\chi_{45\rightarrow46}$ |
| DAMS⁺ | 1→2 | 455 | 1.41 | −13.3 | 0.954 $\chi_{46\rightarrow47}$ |

[a] Expansion of the electronic transition over the excited state orbitals in the configuration interation (CI) formalism. In both cases, there is only one component with a large coefficient. Orbital 45 is the HOMO and 46 is the LUMO in NOMS⁺. Orbital 46 is the HOMO and 47 is the LUMO in DAMS⁺.

experimental values. The calculation gives

$$\beta_{NOMS^+} = 0.171\beta_{DAMS^+}$$

These data are readily related to the electronic transitions involved in the NLO response. Indeed, within the framework of the SOS perturbation theory, the molecular hyperpolarizability can be related to all excited states of the molecule and can be partitioned into two contributions, the so-called two-level ($\beta_2$) and three-level ($\beta_3$) terms.[47] Analysis of term contributions to the molecular hyperpolarizability of "push-pull" chromophores such as DAMS⁺I⁻ indicates that the two-level term usually dominates the nonlinearity. The situation encountered in the case of NOMS⁺ is slightly different, and $\beta_2$ is only slightly higher than $\beta_3$. However, as in a previous similar case,[48] we will make the assumption that three-level terms scale as two-level terms. Therefore, understanding two-level terms should provide qualitative understanding of $\beta$.

INDO-calculated data are reported in Table 10 for the low-lying transition in NOMS⁺I⁻ and in DAMS⁺I⁻. This transition is the only intense band (large oscillator strength) in good agreement with the electronic spectra. The largest oscillator strength has been calculated for NOMS⁺, in agreement with the experimental value. This transitions in both systems principally involves the HOMO → LUMO transition, as indicated by the composition of the configuration interaction. These orbitals are shown in Figure 6 for NOMS⁺ and DAMS⁺, with the difference in electronic population ($LUMO^2 - HOMO^2$) occurring during the transition. The situation encountered for DAMS⁺ is well-understood, with the dimethylamino substituent acting as a strong electron donor. Interestingly, NOMS⁺ exhibits a sizable charge-transfer process in which the phenyl bearing the nitro substituent is the donor and the *N*-methylpyridyl is the acceptor moiety.

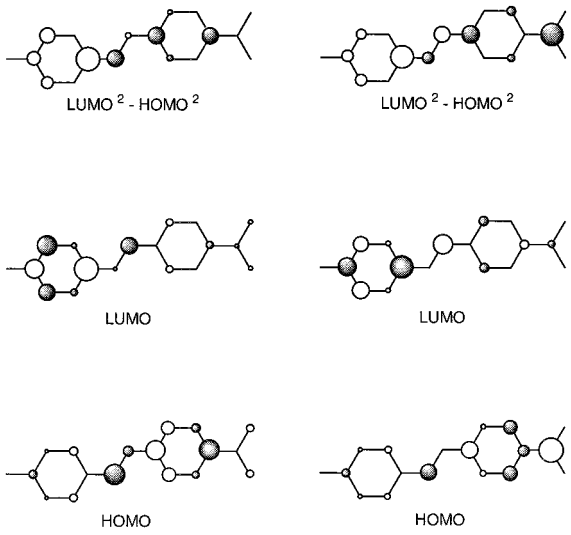


**Figure 6.** Comparison of HOMO, LUMO, and charge transfer ($LUMO^2 - HOMO^2$) for NOMS⁺ (left) and DAMS⁺ (right). For $LUMO^2 - HOMO^2$, the black contribution is indicative of a decrease in electron density in the charge transfer process.

**Hyperpolarizability of NOMS⁺ as a Function of the Oxidation State.** The presence of short distances and $\pi$-overlaps between reducible cationic species and electron-rich anions raises the question of the modification of $\beta$ values as a function of the oxidation state of the chromophore. Evidence for such modification would be desirable if an interplay is expected between NLO and electron delocalization. To date very few investigations have been performed on chromophores with *open-shell* electronic structures. Paramagnetic transition metal complexes have been reported to exhibit large second-order hyperpolarizabilities,[49] and there is evidence that organic radicals could be promising NLO chromophores.[49b,50] However, tuning the NLO response in a charge transfer process is still a challenge, which offers both theoretical and practical interests. It would be of great interest to fully characterize the reduced NOMS⁰ species in order to compare experimental (EFISH) determination of $\beta$ with calculations based on the actual molecular geometry of NOMS⁰. Unfortunately, cyclic voltammetry and coulometry clearly reveal that after a one electron reduction of NOMS⁺ into NOMS⁰, the latter radical undergoes a second reduction process to NOMS⁻. The stability of NOMS⁰ depends on the comproportionation constant ($K_{con}$), calculated for the equilibrium

$$NOMS^- + NOMS^+ \overset{K_{con}}{\rightleftharpoons} 2NOMS^0$$

with the potentials for the two reduction waves being as follows: $E_2 - E_1 = 0.059 \log(K_{con})$. It can be seen from the above relations that the intermediate oxidation

(47) See for example: (a) Kanis, D. R.; Ratner, M. A.; Marks, T. J. *J. Am. Chem. Soc.* **1992**, *114*, 10338. (b) Di Bella, S.; Fragalà, I.; Ledoux, I.; Marks, T. J. *J. Am. Chem. Soc.* **1995**, *117*, 9481.

(48) Kanis, D. R.; Lacroix, P. G.; Ratner, M. A. Marks, T. J. *J. Am. Chem. Soc.* **1994**, *116*, 10089.

(49) (a) Di Bella, S.; Fragalà, I.; Ledoux, I.; Marks, T. J. *J. Am. Chem. Soc.* **1995**, *117*, 9481. (b) Di Bella, S.; Fragalà, I.; Marks, T. J.; Ratner, M. A. *J. Am. Chem. Soc.* **1996**, *118*, 12747. (c) Lacroix, P. G.; Di Bella, S.; Ledoux, I. *Chem. Mater.* **1996**, *8*, 541

(50) (a) Yam, R.; Cohen, R.; Berkovic, G. *Nonlinear Opt.* **1995**, *11*, 311. (b) Lundquist, P. M.; Yitzchaik, S.; Marks, T. J.; Wong, G. K.; Di Bella, S.; Cohen, R.; Berkovic, G. *Phys. Rev. B*, in press

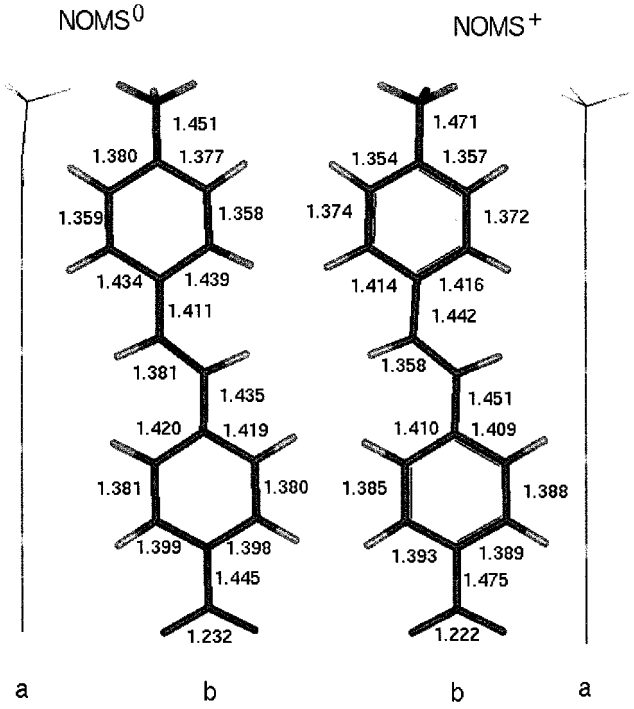


**Figure 7.** Side view (a) and front view (b) of the molecular structure for $NOMS^0$ and $NOMS^+$ calculated with the DFT method.

state ($NOMS^0$) can be isolated only if $E_2$ and $E_1$ are significantly different. The small change in wave separation (71 mV) leads to a very small comproportionation constant ($K_{con} = 0.063$). Consequently, $NOMS^0$ cannot be isolated and characterized. Therefore, only a theoretical investigation will be presented here.

Starting from the X-ray diffraction structure of $NOMS^+$ in $[NOMS][Ni(dmit)_2]$, the gas-phase structures of $NOMS^0$ and $NOMS^+$ have been calculated at the B3PW91/6-31G* level and are compared in Figure 7. Working on the gas phase is of prime importance, to avoid the effect of the environment on the molecular structure, and hence on the hyperpolarizability.[51] Therefore, comparing the calculations will account for the effect of the charge only. In the calculated structures, the *p*-nitrophenyl and *N*-methylpyridyl rings are coplanar, in contrast to the angle of 7.1° observed between both rings in the crystal structure of $[NOMS][Ni(dmit)_2]$. The latter distortion may be induced by strong intermolecular interactions suggested by the short S···C contacts observed in the crystal packing of $(NOMS)[Ni(dmit)_2]$.

The bond length modifications (Figure 7) resulting from the reduction of $NOMS^+$ into $NOMS^0$ are consistent with a quinoidal transformation of the rings and a decrease of the aromatic character, which are more pronounced for the *N*-methylpyridyl moiety. The out of plane displacement of the methyl group after reduction is additional evidence of this phenomenon. Indeed, the angle between $CH_3-N$ and the pyridyl plane, which is equal to 0.1° in the calculated structure of $NOMS^+$ (in agreement with the $sp^2$ hybridation of the nitrogen),

(51) (a) Di Bella, S.; Fragalà, I.; Ratner, M. A.; Marks, T. J. *Chem. Mater.* **1995**, *7*, 400. (b) Di Bella S.; Marks T. J.; Ratner M. A. *J. Am. Chem. Soc.* **1994**, *116*, 4440. (c) Di Bella S.; Ratner M. A.; Marks T. J. *J. Am. Chem. Soc.* **1992**, *114*, 5842.

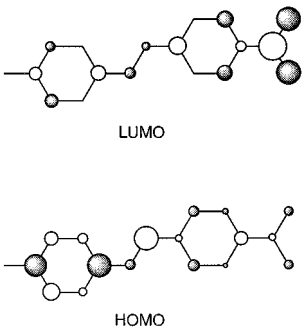


**Figure 8.** Frontier orbitals of $NOMS^0$.

**Scheme 2**

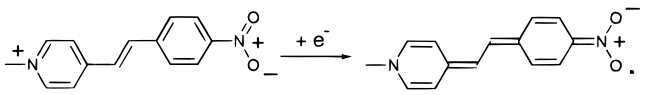


becomes 7.3° in $NOMS^0$ after reduction. All the above geometric modifications observed upon reduction of $NOMS^+$ are in agreement with the resonant structure of $NOMS^0$ shown in Scheme 2.

The frontier orbitals topologies predicted by semiempirical or DFT methods are in complete agreement and are schematically depicted in Figure 8 for $NOMS^0$. The atomic coefficients of the LUMO of $NOMS^+$ are larger on the *N*-methylpyridinium moiety of the chromophore. This suggests that this moiety should bear most of the electron density, once $NOMS^+$ has been reduced into $NOMS^0$. Moreover, this is in agreement with the important geometry transformations observed for the *N*-methyl-pyridyl fragment.

When the HOMO → LUMO transition of $NOMS^0$ is compared to the one of $NOMS^+$, the most striking feature is the reverse charge transfer occurring after reduction, which suggests a change in the sign of $\beta$, from negative to positive values. We can therefore suggest that partial reduction of $NOMS^+$ by $[Ni(dmit)_2]^-$ should reduce the intramolecular charge transfer and, hence, the hyperpolarizability of $NOMS^{\delta+}$ ($\delta < 1$). However, as more electron density is being transferred, an intramolecular charge transfer would take place in $NOMS^{\delta'+}$ ($\delta' < \delta$) from the *N*-methylpyridyl part toward the *p*-nitrophenyl-part of the molecule, resulting in a positive $\beta$ value.

Unfortunatly, the first-order hyperpolarizability of $NOMS^0$ cannot be evaluated using the SOS formalism of our ZINDO release because calculation of open-shell chromophores is not available. We have therefore compared the static hyperpolarizability [$\beta_{(0)}$] of $NOMS^+$ and $NOMS^0$ determined using either the numerical finite field procedure included in MOPAC (PM3) and in Gaussian94 (B3PW91/6-31G* level) or the analytic coupled perturbed Hartree−Fock procedure (HF/6-31G* level) available in Gaussian94. The scope and limitation of these methodologies has been reviewed.[28] The calculated hyperpolarizabilities values are gathered in Table 11. It is noteworthy that significant differences in the magnitude of the hyperpolarizabilities are observed, depending on the calculation methods. Ab initio-CPHF computations of static hyperpolarizabilities are expected to be more accurate than semiempirical CPHF methodologies such as the one included in MOPAC. Nevertheless, they are sensitive to the treatment of electron

**Table 11. Hyperpolarizabilities of NOMS$^+$ and NOMS$^0$ Calculated with Different Quantum Chemical Approaches**

| | | molecular hyperpolarizability ($\beta$) | | | |
|---|---|---|---|---|---|
| | | Gaussian (6-31G*) | | MOPAC | |
| compd | geometry | CPHF HF | FF B3PW91 | FF PM3 | ZINDO SOS |
| NOMS$^+$ | crystallography | −34.9 | −71.9 | −72.8 | −16.7 |
| NOMS$^+$ | GAUSSIAN | −43.5 | −63.5 | −95.5 | −20.0 |
| NOMS$^0$ | GAUSSIAN | 84.8 | 200.6 | 203.3 | na[a] |

[a] Data non available.

correlation. This may explain the difference between CPHF/HF-6-31G* (no electron correlation) and FF-B3PW91/6-31G* (DFT electron correlation included) $\beta$ calculations. The fact that the first method involves analytical derivatization of the energy versus the electric field, whereas derivatives are numerically computed in the second method, may also account for the different $\beta$ values given by the two ab initio CPHF computations (Table 11).

Beyond the differences in the magnitude of $\beta$, the same general trends are observed, whatever the method used: (i) the sign of $\beta$ is changed upon reduction, in agreement with the above frontier orbitals analysis, and (ii) there is a significant increase of $\beta$ upon reduction of NOMS$^+$ into NOMS$^0$, $\beta_{\text{NOMS}^0}$ being about twice as large as $|\beta_{\text{NOMS}^+}|$. To verify the actual effect of the chromophore environement, which seems to be important owing to the seven van der Waals short distances observed in (NOMS)$^+$[Ni(dmit)$_2$]$^-$, direct hyperpolarizability measurements of NOMS$^+$ in different crystal environements (e.g. $PF_6^-$ and [Ni(dmit)$_2$]$^-$) could be performed. Although such an experiment was not the purpose of the present investigation, it could give interesting ideas on the actual effect of anion−cation interactions in the solid state.

## Conclusion

Contrary to DAMS$^+$, which is one of the best second-order NLO chromophores, NOMS$^+$ undergoes reduced, but still sizable, noncentrosymmetric charge transfer. However, both cations, which have very similar molecular shapes, give salts with [Ni(dmit)$_2$]$^-$ exhibiting similar overall structural arrangements. The main difference is observed in the molecular stacking of the chromophores with respect to the [Ni(dmit)$_2$]$^-$ slabs. This last point, which seems to be related to the redox potential of the cations, may offer a key toward efficient interplays between NLO and conducting properties in molecular materials. This study has provided evidence for the possibility of tunable molecular NLO responses through intermolecular charge transfers. The computations provide additional evidence on the use of organic radicals such as NOMS$^0$ in the design of chromophores with sizable hyperpolarizability.[49b]

**Acknowledgment.** The authors thank Dr. de Montauzon for the electrochemical measurement, and Dr. P. Cassoux for stimulating discussions.

**Supporting Information Available:** Tables of crystal data for [Ni(dmit)$_2$]$^-$(NOMS$^+$) (6 pages). Ordering information is given on any current masthead page.

CM980487Z